

Article

Effect of Thermomechanical Cycling on Martensitic Transformation and Shape Memory Effect in 304 Austenitic Steel

Jie Chen ¹, Yonghao Zhang ¹, Jiqiang Ge ¹, Huabei Peng ², Shuke Huang ¹, Qin Yang ^{1,*} and Yuhua Wen ^{2,*}

¹ Institute of Machinery Manufacturing Technology, China Academy of Engineering Physics, Mianyang 621900, China; jiechen_6s@caep.cn (J.C.); kevear@foxmail.com (Y.Z.); Gejiqiang@126.com (J.G.); huangshuke@163.com (S.H.)

² School of Mechanical Engineering, Sichuan University, Chengdu 610065, China; penghuabei2002@126.com

* Correspondence: yangqin_6s@caep.cn (Q.Y.); wenyh@scu.edu.cn (Y.W.); Tel.: +86-0816-248-7629 (Q.Y.)

Received: 7 June 2020; Accepted: 1 July 2020; Published: 6 July 2020



Abstract: To improve the shape memory effect (SME) of 304 austenitic steel effectively and efficiently, thermomechanical cycling, comprising deformation at room temperature and annealing, was applied. The influences of cycle number and annealing temperature on the SME and microstructures in 304 austenitic steel were investigated by light microscope (LM), X-ray diffraction (XRD), and transmission electron microscope (TEM). The shape recovery ratio was remarkably improved from 16% to 40% after two thermomechanical cycles. The optimum annealing temperature was 833 K in the process of thermomechanical cycling. The improved SME by thermomechanical cycling was mainly related to stress-induced ϵ martensite rather than stress-induced α' martensite. The reason is that thermomechanical cycling can not only promote the occurrence of the stress-induced $\gamma \rightarrow \epsilon$ martensitic transformation, but also suppress the subsequently stress-induced $\epsilon \rightarrow \alpha'$ transformation.

Keywords: austenitic steel; thermomechanical cycling; martensitic transformation; shape memory effect

1. Introduction

Because of its good mechanical properties, corrosion resistance, and weldability, 304 austenitic steel is widely used in civil engineering applications [1]. It is well known that the metastable γ austenite in 304 austenitic steel can transform into ϵ martensite and/or α' martensite [2,3]. Enami et al. reported that, as a result of the stress-induced $\gamma \rightarrow \epsilon$ martensitic transformation and its reverse transformation, a weak shape memory effect (SME) occurred in 304 austenitic steel [4,5]. In contrast, a good SME could be obtained in FeMnSi-based alloys resulting from the stress-induced $\gamma \rightarrow \epsilon$ martensitic transformation [6–11]. Considering the superior corrosion resistance and workability of 304 austenitic steel, it is significant to improve the SME resulting from the stress-induced $\gamma \rightarrow \epsilon$ martensitic transformation in 304 austenitic steel.

Thermomechanical cycling can significantly improve the SME of FeMnSi-based alloys. Here, thermomechanical cycling consists of several cycles of tensile deformation at room temperature (RT) and the subsequent annealing (simply recorded as thermomechanical cycling at RT) [12–15]. The essence of thermomechanical cycling is the repetition of the stress-induced $\gamma \rightarrow \epsilon$ martensitic transformation and its reverse transformation. Mangonon et al. reported that such a repetition can also occur in 304 austenitic steel when deformed at subzero temperatures and after subsequent annealing [16]. However, they had not investigated the effect of thermomechanical cycling at subzero temperatures on the SME in 304 austenitic steel. Recently, Chen et al. reported that the recovered strain of 304 austenitic

steel was improved to 1% by thermomechanical cycling comprising tensile deformation at 178 K and subsequent annealing (simply recorded as thermomechanical cycling at 178 K) [17]. Watanabe et al. reported that, through embedding the FeMnSi-based wires with only 1% recovered strain into a plaster matrix, the fracture toughness of plaster can be effectively improved [18]. Therefore, it can be expected that 304 austenitic steel with 1% recovered strain will have potential engineering applications in the architectural and civil engineering industry.

We note that it will be more efficient and cost effective if thermomechanical cycling at RT can improve the SME of 304 austenitic steel as well as thermomechanical cycling at 178 K. Nevertheless, the martensitic transformation of 304 austenitic steel changes from $\gamma \rightarrow \varepsilon$ to $\gamma \rightarrow \alpha'$ and/or to $\gamma \rightarrow \varepsilon \rightarrow \alpha'$ as the deformation temperature rises from subzero temperatures to RT [19–23]. It is not clear whether the thermomechanical cycling at RT is suitable to improve the SME of 304 austenitic steel, due to the absence of $\gamma \rightarrow \varepsilon$ martensitic transformation. In this study, we investigate the effects of thermomechanical cycling comprising 13% tensile deformation at RT and subsequent annealing at different temperatures on the SME and microstructures of 304 austenitic steel, in order to investigate the aforementioned issues. The results demonstrate that the SME of 304 austenitic steel can be effectively and efficiently improved by thermomechanical cycling at RT, which can be used as a shape memory alloy in the architectural and civil engineering industry.

2. Materials and Methods

The composition of 304 austenitic steel used in the present paper was 18.12Cr, 8.16Ni, 1.51Mn, 0.53Si, 0.11V, 0.04Cu, 0.02P, 0.04C (wt. %), and balance Fe. Dog-bone-shaped specimens with gauge dimensions of $80 \times 5 \times 2 \text{ mm}^3$ were cut from sheets by electric discharge machining. All the specimens were solution treated at 1353 K for 30 min and then air cooled to RT. Some specimens were further subjected to thermomechanical cycling consisting of 13% tensile strain at RT and subsequent annealing at different temperatures for 30 min. Specimens of $60.0 \times 1.5 \times 2.0 \text{ mm}^3$ for SME measurements were cut from dog-bone-shaped specimens subjected to thermomechanical cycling. The shape recovery ratio (SRR) and the recovered strain in the SME measurement were calculated according to conventional bend testing [24]. After the measurement, the specimens were deformed at 77 K after being maintained for 5 min, and then they were directly heated at 1073 K or step-heated at different temperatures up to 1073 K. The 0.2% proof stress $\sigma_{0.2}$ at different temperatures was determined from the tensile stress–strain curves. The values of the $\sigma_{0.2}$ were the average of three tensile measurements.

The microstructure was investigated by light microscope (LM), X-ray diffraction (XRD), and transmission electron microscope (TEM). The LM observations were performed using a GX51 microscope (Olympus, Tokyo, Japan). The specimens were mechanically ground and electro-polished in a solution of 90% $\text{C}_2\text{H}_5\text{OH}$ and 10% HClO_4 . Subsequently, an optical etchant comprising 0.5% NH_4HF_2 and 1.2% $\text{K}_2\text{S}_2\text{O}_5$ in water was used. The XRD measurements were carried out on the X' Pert Pro MPD X-ray diffraction apparatus (Philips, Almelo, The Netherlands) using Cu target with the scanning rate of 6° min^{-1} . The TEM measurements were performed using a Tecnai F20 transmission electron microscope (FEI, Hillsboro, OR, USA). Thin foils were mechanically ground and then polished in a solution of 20% H_2SO_4 and 80% CH_3OH using a twin jet polisher (Shanghai Jiaoda Ltd., Shanghai, China).

3. Results

3.1. Shape Memory Effect

Figure 1 depicts the SRR of specimens subjected to one thermomechanical cycle comprising 13% tensile strain at RT and subsequent annealing at different temperatures. The SRR was calculated when the thermomechanically treated specimens were bent by 2.5% at 77 K and then directly heated at 1073 K. As the annealing temperature increased, the SRR rose from 16% to 24% until the annealing temperature reached 833 K, after which it dropped to 19% as the temperature reached 1073 K. Thus, the optimized annealing temperature in the process of thermomechanical cycling was 833 K.

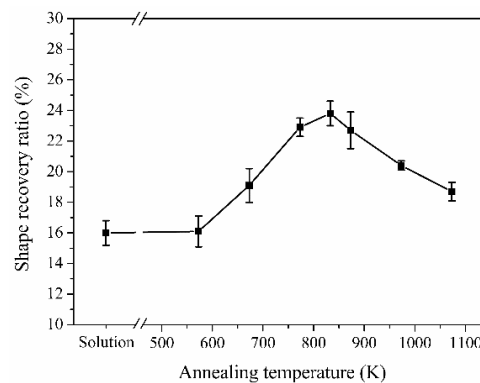


Figure 1. Effect of annealing temperature in one thermomechanical cycle on shape recovery ratio for specimens after being bent by 2.5% at 77 K and then directly heated at 1073 K.

The effect of thermomechanical cycle number on the SRR is shown in Figure 2. Each thermomechanical cycle consists of 13% tensile strain at RT and subsequent annealing at 833 K (here and after). The SRR was calculated when the thermomechanically treated specimens were bent by 2.5% at 77 K and then directly heated at 1073 K. The SRR significantly increased from 16% to 40% after two thermomechanical cycles. When further increasing the thermomechanical cycle number, the SRR remained almost unchanged at around 40%.

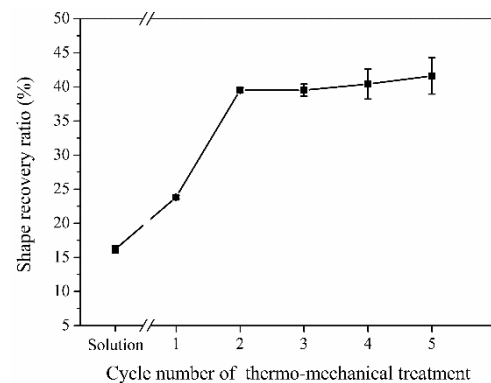


Figure 2. Effect of thermomechanical cycle number on shape recovery ratio for specimens after being bent by 2.5% at 77 K and then directly heated at 1073 K. Each thermomechanical cycle consists of 13% tensile strain at RT and subsequent annealing at 833 K.

Figure 3 compares the recovered strains of the solution-treated specimen and the one subjected to two thermomechanical cycles after 2.5% strain and 10% strain at 77 K. Here, the SRR was calculated after the strained specimen was step-heated to 1073 K. When deformed by 2.5%, weak two-stage recoveries can be observed below 473 K and above 773 K for the solution-treated specimen (black line in Figure 3a). After two thermomechanical cycles, the recovered strain significantly increased from 77 K to 473 K, and then it increased slightly with the increase in the temperature (red line in Figure 3a). When deformed by 10%, two-stage recoveries can be observed below 523 K and above 673 K for both the solution-treated specimen and the one subjected to two thermomechanical cycles (Figure 3b). Similarly, the increase in the recovered strain for the 10% strained specimen was observed mainly below 523 K instead of above 673 K.

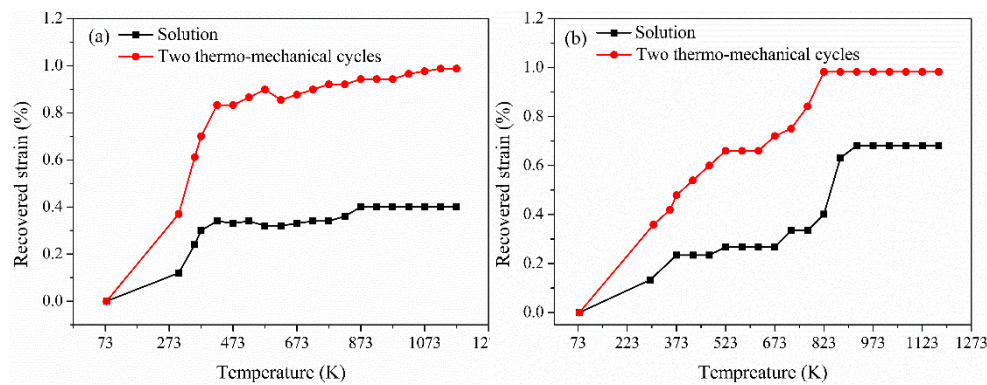


Figure 3. Recovered strains of solution-treated specimen and the one subjected to two thermomechanical cycles as a function of step-heating temperatures after 2.5% strain (a) and 10% strain (b) at 77 K.

3.2. Microstructures and Mechanical Behavior

The LM images after deep cooling at 77 K for the specimens subjected to solution treatment and two thermomechanical cycles are shown in Figure 4a,c. It can be observed that the LM images for the solution-treated and thermomechanically treated specimens were quite different. Compared to the solution-treated specimen, numerous clusters of black phase occurred in the thermomechanically treated specimen (Figure 4c). The XRD pattern confirmed that no diffraction peak of α' martensite was identified in the solution-treated specimen (Figure 4b). In contrast, the XRD pattern for the specimen subjected to two thermomechanical cycles revealed that some diffraction peaks of (110), (200), and (211) for the α' martensite appeared (Figure 4d). Therefore, it is very likely that the clusters of black phase in Figure 4c are actually numerous small units of α' martensite.

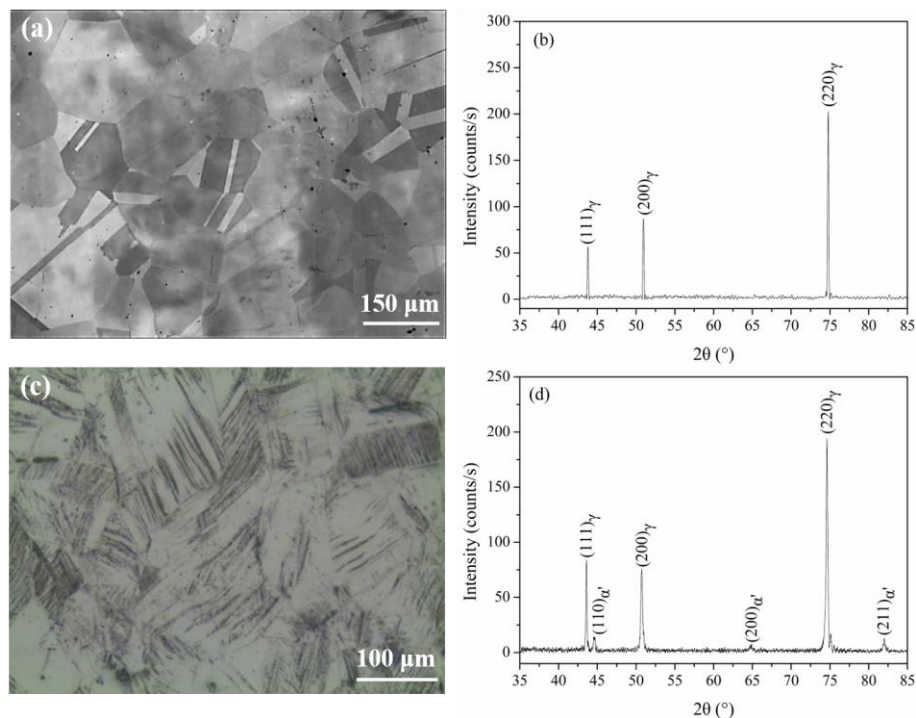


Figure 4. Microstructures of the solution-treated specimen and the one subjected to two thermomechanical cycles: (a) light microscope (LM) image and (b) X-ray diffraction (XRD) pattern of solution-treated specimen; (c) LM image and (d) XRD pattern of that after two thermomechanical cycles.

Figure 5 presents the TEM microstructures for the specimens subjected to solution treatment and two thermomechanical cycles. Only a few stacking faults were observed for the solution-treated specimen (Figure 5a). In contrast, a large number of dislocations were observed in the specimen after two thermomechanical cycles (Figure 5b). Meanwhile, a few residual α' martensite particles can also be observed (Figure 5c).

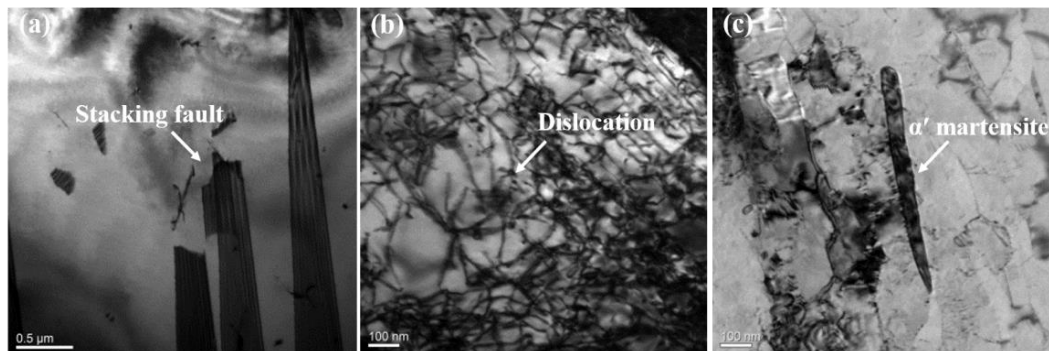


Figure 5. Transmission electron microscope (TEM) microstructures of solution-treated specimen (a) and the one subjected to two thermomechanical cycles (b,c).

Figure 6 exhibits the TEM microstructures of the solution-treated specimen after 2.5% strain at 77 K. Some thick ϵ martensite laths can be observed in Figure 6a,b. Additionally, the black phase with lenticular shape can be clearly observed in the dark-field image using $(10\bar{1}0)\epsilon$ reflection (Figure 6c). The selected-area diffraction pattern revealed that the black phase was α' martensite (Figure 6d).

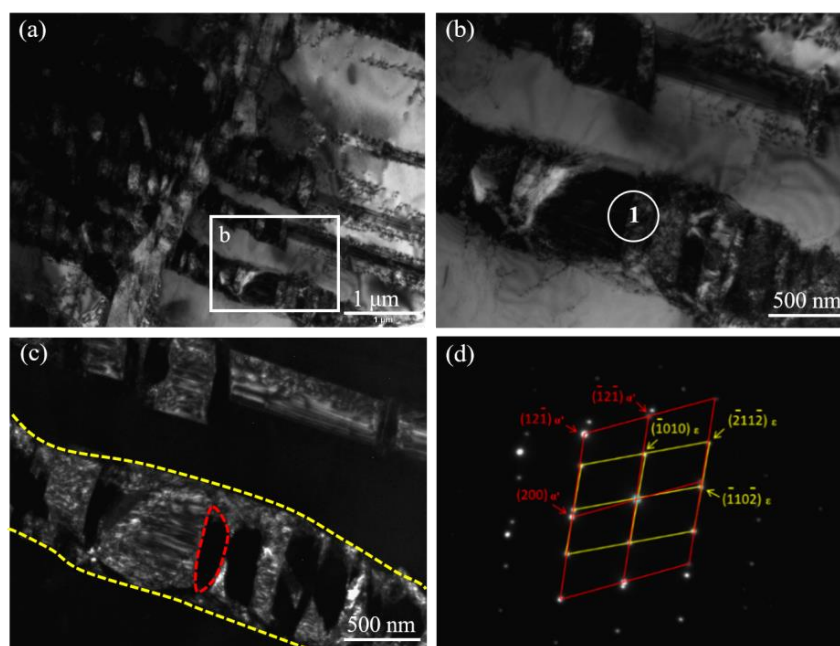


Figure 6. TEM microstructures of solution-treated specimen after 2.5% strain at 77 K: (a) bright-field image; (b) enlarged image of area b in (a); (c) dark-field image using $(10\bar{1}0)\epsilon$ reflection; (d) selected-area diffraction pattern corresponding to area 1 shown in (b), zone axis = $[24\ 2\bar{3}]\epsilon$, zone axis = $[12]\alpha'$.

Figure 7 displays the TEM microstructures of the specimen subjected to two thermomechanical cycles after 2.5% strain at 77 K. Some very thin and straight laths can be observed in Figure 7a, and the black phase can be hardly observed inside the laths (Figure 7b,c). The selected-area diffraction pattern (Figure 7d) revealed that the thin lath was ϵ martensite. The ϵ martensite orientation relationship with the matrix is in accordance with the S–N relationship, i.e., $[2\bar{1}\bar{1}0]\epsilon // [01\bar{1}]\gamma$, $(0001)\epsilon // (111)\gamma$.

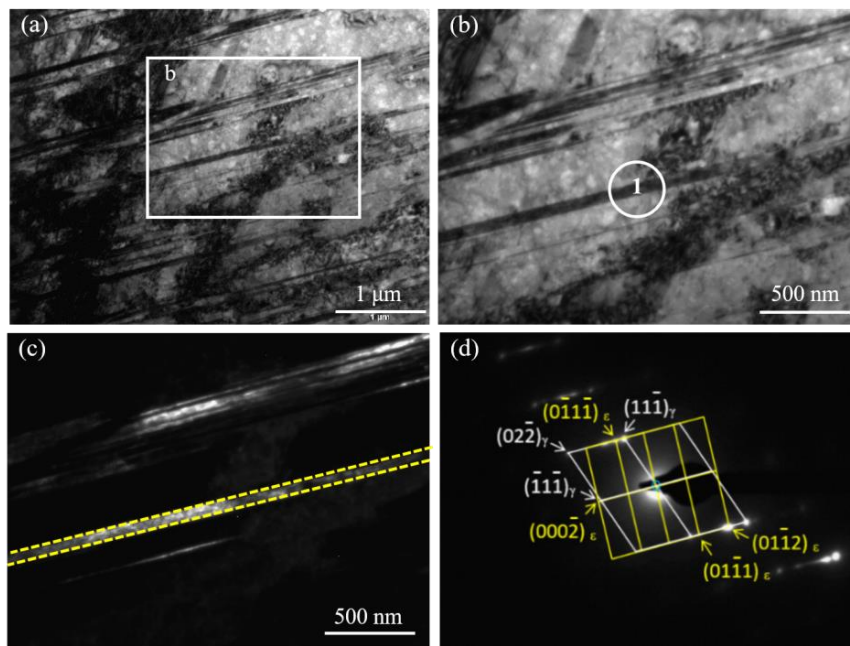


Figure 7. TEM microstructures of the specimen subjected to two thermomechanical cycles after 2.5% strain at 77 K: (a) bright-field image; (b) enlarged image of area b in (a); (c) dark-field image using $(0\bar{1}\bar{1})_{\epsilon}$ reflection; (d) selected-area diffraction pattern corresponding to area 1 shown in (a), zone axis = $[2\bar{1}\bar{1}\ 0]_{\epsilon}$, zone axis = $[0\bar{1}\bar{1}]_{\gamma}$.

Figure 8 illustrates the 0.2% proof stress $\sigma_{0.2}$ as a function of deformation temperatures for the solution-treated specimen and the one subjected to two thermomechanical cycles. For the solution-treated specimens, only a weak positive temperature dependence of the $\sigma_{0.2}$ was observed between 123 K and 223 K. For the specimens subjected to two thermomechanical cycles, an obvious positive temperature dependence of the $\sigma_{0.2}$ existed at the region between 77 K and 273 K. Note that the $\sigma_{0.2}$ of the thermomechanically treated specimens was obviously much higher than that of the solution-treated ones.

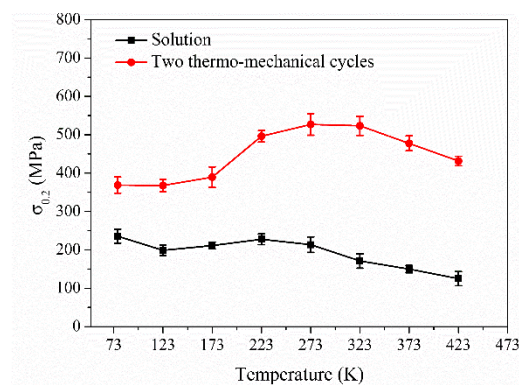


Figure 8. The 0.2% proof stress $\sigma_{0.2}$ as a function of temperatures for solution-treated specimens and the ones subjected to two thermomechanical cycles.

4. Discussion

4.1. Improving SME Related to Stress-Induced ϵ Martensite by Thermomechanical Cycling

Recently, Wang et al. reported that the occurrence of both stress-induced ϵ martensite and α' martensite could result in the SME of 304 austenitic steel [25]. They proposed that the SME related to stress-induced ϵ martensite occurred when the heating temperature was below 473 K, while the SME

related to stress-induced α' martensite occurred above 873 K. Herein, the increase in the recovered strain by thermomechanical cycling mainly occurred when the heating temperature was below 473 K rather than above 673 K (Figure 3). This indicates that the SME related to stress-induced ε martensite, rather than stress-induced α' martensite, was enhanced by thermomechanical cycling in 304 austenitic steel.

Therefore, to improve the SME related to stress-induced ε martensite in 304 austenitic steel, the stress-induced $\gamma \rightarrow \varepsilon$ transformation should be promoted as far as possible. Simultaneously, the subsequently stress-induced $\varepsilon \rightarrow \alpha'$ transformation should be suppressed. As a result of the suppression of the stress-induced $\varepsilon \rightarrow \alpha'$ transformation, more stress-induced ε martensite can be maintained after deformation. Meanwhile, the reversibility of stress-induced ε reverse transformation could be enhanced by weakening the pinning effect of the α' martensite on the stress-induced ε martensite.

4.2. Promoting Effect of Thermomechanical Cycling on Stress-Induced $\gamma \rightarrow \varepsilon$ Transformation

Although stress-induced $\gamma \rightarrow \varepsilon$ transformation can occur in 304 austenitic steel, only a weak positive temperature dependence of the $\sigma_{0.2}$ occurred in the solution-treated specimens (Figure 8). This demonstrates that the matrix strength of 304 austenitic steel is too low, and it is hard to distinguish the stress-induced ε martensitic transformation from the onset of permanent slip. That is to say, the stress-induced $\gamma \rightarrow \varepsilon$ transformation and permanent slip in the solution-treated specimens occurred simultaneously during deformation.

Chen et al. claimed that numerous stacking faults and residual α' martensite were introduced in 304 austenitic steel after thermomechanical cycling at 178 K [17]. The numerous stacking faults can act as nucleation of the stress-induced ε martensite, and thus lower the critical stress for the stress-induced $\gamma \rightarrow \varepsilon$ transformation. On the other hand, the large amount of residual α' martensite can significantly increase the critical stress for permanent slip and thus strengthen the matrix. Compared with the specimen after thermomechanical cycling at 178 K, the microstructure is significantly different after thermomechanical cycling at RT in the one in this study. Specifically, a large density of dislocations and a few residual α' martensite units can be observed in the specimen after thermomechanical cycling at RT (Figure 5b,c), while stacking faults can hardly be observed. Such a difference can be attributed to the fact that permanent slip becomes the main deformation mode when increasing the deformation temperature from 178 K to RT in thermomechanical cycling. Interestingly, though stacking faults are rarely introduced, the stress-induced $\gamma \rightarrow \varepsilon$ martensitic transformation can still effectively be promoted owing to the large density of dislocations introduced in thermomechanical cycling at RT. As shown in Figure 8, an obvious negative temperature dependence of the $\sigma_{0.2}$ appeared at the region between 77 K and 273 K in the thermomechanically treated ones. This phenomenon indicates that more shape change can be assumed by the stress-induced $\gamma \rightarrow \varepsilon$ transformation in the thermomechanically treated specimens. When the annealing temperature in the thermomechanical cycling was rather low, too many dislocations would impede the stress-induced $\gamma \rightarrow \varepsilon$ transformation. When the annealing temperature was rather high, dislocations would disappear as a result of the recrystallization. Consequently, an optimal annealing temperature of 833 K existed for the improved SME in the thermomechanically treated 304 austenitic steel (Figure 1).

4.3. Suppressing Effect of Thermomechanical Cycling on Stress-Induced $\varepsilon \rightarrow \alpha'$ Transformation

It is generally accepted that ε martensite can act as the precursory phase of the α' martensite, i.e., the $\gamma \rightarrow \varepsilon \rightarrow \alpha'$ transformation routine. For instance, Kruml et al. [26] and Lee et al. [27] observed that the α' martensite can be produced at the intersections of ε martensite or in a single ε martensite phase. In addition, the α' martensite can be directly transformed from γ austenite phase at the austenite grain boundary, i.e., the $\gamma \rightarrow \alpha'$ transformation routine [28]. Herein, small units of α' martensite can be easily observed inside the individual ε martensite bands in the solution-treated specimen after deformation at 77 K (Figure 6), indicating the existence of the $\gamma \rightarrow \varepsilon \rightarrow \alpha'$ transformation routine. This indicates that the stress-induced ε martensite can easily transform into α' martensite in 304 austenitic steel, due to the lower stability of the ε martensite than the α' martensite. Moreover, the stress-induced ε martensite

can be pinned by the small α' martensite inside, thereby impeding the reverse transformation of ε martensite upon heating.

Dai et al. reported that the martensitic transformation sequence could be changed by both the yield strength ($\sigma_{0.2}$) and stacking fault energy (γ_{SF}) in austenitic steels [29]. They proposed that the formation of stress-induced ε martensite was more favorable with the decrease in the value of structural parameter $S = \gamma_{SF}/(\sigma_{0.2} \cdot b)$, whereas the amount of stress-induced α' martensite produced would be less. Herein, as a result of the significant enhancement of $\sigma_{0.2}$ by thermomechanical cycling at RT, the structural parameter S of 304 austenitic steel was expected to decrease. Consequently, the stress-induced $\varepsilon \rightarrow \alpha'$ transformation could be suppressed. As shown in Figure 7, the α' martensite can hardly be observed inside the stress-induced ε martensite in the thermomechanically treated specimen after deformation, which confirmed this. Owing to the suppression of stress-induced $\varepsilon \rightarrow \alpha'$ transformation, more stress-induced ε martensite can be maintained and its reversibility can be promoted.

5. Conclusions

(1) The SME of 304 austenitic steel can be significantly improved by thermomechanical cycling, consisting of 13% strain at room temperature and subsequent annealing at 833 K. After two thermomechanical cycles, the SME increased from 16% to 40%. The excessive thermomechanical cycles cannot further improve the SME;

(2) Thermomechanical cycling at room temperature mainly enhances the SME related to the stress-induced ε martensite rather than stress-induced α' martensite in 304 austenitic steel;

(3) Thermomechanical cycling at room temperature can not only promote the occurrence of the stress-induced $\gamma \rightarrow \varepsilon$ martensitic transformation, but also suppress the subsequently stress-induced $\varepsilon \rightarrow \alpha'$ transformation.

Author Contributions: Conceptualization and writing—original draft, J.C.; methodology, H.P.; formal analysis, Y.Z.; resources and validation, S.H.; data curation, J.G.; writing—review and editing, Q.Y.; supervision, Y.W. All authors have read and agreed to the published version of the manuscript.

Funding: This research was funded by National Natural Science Foundation of China (grant number 51901214), the CAEP Foundation (grant number CX20200013), and National Safety Academic Fund (grant number U1930207).

Conflicts of Interest: The authors declare no conflict of interest.

References

- Lo, K.H.; Shek, C.H.; Lai, J.K.L. Recent developments in stainless steels. *Mater. Sci. Eng. R* **2009**, *65*, 39–104. [[CrossRef](#)]
- Unnikrishnan, R.; SatishIdury, K.S.N.; Ismail, T.P.; Bhadauria, A.; Shekhawat, S.K.; Khatirkar, R.K.; Sapate, S.G. Effect of heat input on the microstructure, residual stresses and corrosion resistance of 304L austenitic stainless steel weldments. *Mater. Charact.* **2014**, *93*, 10–23. [[CrossRef](#)]
- Mangonon, P.L., Jr.; Thomas, G. Martensite phases in 340 stainless steel. *Metall Trans.* **1970**, *1*, 1577–1586. [[CrossRef](#)]
- Enami, K.; Nenno, S.; Minato, Y. Shape memory effect associated with the martensite transformation in 304 type stainless steel. *Scr. Metall.* **1971**, *5*, 663–667. [[CrossRef](#)]
- Enami, K.; Nenno, S.; Minato, Y. Direct observations of the reverse transformation of ε martensite in type 304 stainless steel. *Trans. JIM* **1977**, *18*, 435–442. [[CrossRef](#)]
- Sato, A.; Chishima, E.; Soma, K.; Mori, T. Shape memory effect in $\gamma \rightarrow \varepsilon$ transformation in Fe-30Mn-1Si alloy single crystals. *Acta Metall.* **1982**, *30*, 1177–1183. [[CrossRef](#)]
- Wen, Y.H.; Peng, H.B.; Raabe, D.; Gutiérrez-Urrutia, I.; Chen, J.; Du, Y.Y. Large recovery strain in Fe-Mn-Si-based shape memory steels obtained by engineering annealing twin boundaries. *Nat. Commun.* **2014**, *5*, 4964. [[CrossRef](#)] [[PubMed](#)]
- Kajiwara, S. Characteristic features of shape memory effect and related transformation behavior in Fe-based alloys. *Mater. Sci. Eng. A* **1999**, *273*, 67–88. [[CrossRef](#)]

9. Peng, H.B.; Chen, J.; Wang, Y.N.; Wen, Y.H. Key factors achieving large recovery strains in polycrystalline Fe-Mn-Si-based shape memory alloys: A review. *Adv. Eng. Mater.* **2018**, *1700741*, 1–18. [[CrossRef](#)]
10. Tomota, Y.; Nakagawara, W.; Tsuzaki, K.; Maki, T. Reversion of stress-induced ϵ martensite and two-way shape memory in Fe-24Mn and Fe-24Mn-6Si alloys. *Scr. Metall. Mater.* **1992**, *26*, 1571–1574. [[CrossRef](#)]
11. Peng, H.B.; Wang, G.X.; Wang, S.L.; Chen, J.; MacLaren, I.; Wen, Y.H. Key criterion for achieving giant recovery strains in polycrystalline Fe-Mn-Si based shape memory alloys. *Mater. Sci. Eng. A* **2018**, *712*, 37–49. [[CrossRef](#)]
12. Peng, H.B.; Wen, Y.H.; Liu, G.; Wang, C.P.; Li, N. A role of α' martensite introduced by thermo-mechanical treatment in improving shape memory effect of an Fe-Mn-Si-Cr-Ni alloy. *Adv. Eng. Mater.* **2011**, *13*, 388–394. [[CrossRef](#)]
13. Reyhani, M.M.; McCormick, P.G. Effect of thermomechanical cycling in an Fe-Mn-Si-Cr-Ni shape memory alloy. *Scr. Metall. Mater.* **1994**, *31*, 875–878. [[CrossRef](#)]
14. Stanford, N.; Dunne, D.P. Thermo-mechanical processing and the shape memory effect in an Fe-Mn-Si-based shape memory alloy. *Mater. Sci. Eng. A* **2006**, *422*, 352–359. [[CrossRef](#)]
15. Druker, A.; Baruj, A.; Malarría, J. Effect of rolling conditions on the structure and shape memory properties of Fe-Mn-Si alloys. *Mater. Charact.* **2010**, *61*, 603–612. [[CrossRef](#)]
16. Mangonon, P.L.; Thomas, G. Structure and properties of thermal-mechanically treated 304 stainless steel. *Metall. Trans.* **1970**, *1*, 1587–1594. [[CrossRef](#)]
17. Chen, J.; Peng, H.B.; Wang, S.L.; Du, Y.Y.; Wen, Y.H. Remarkable improvement of shape memory effect in austenitic stainless steel by thermo-mechanical training. *Adv. Eng. Mater.* **2015**, *17*, 330–333. [[CrossRef](#)]
18. Watanabe, Y.; Miyazaki, E.; Okada, H. Smart materials-fundamentals and applications. Enhanced mechanical properties of Fe-Mn-Si-Cr shape memory fiber/plaster smart composite. *Mater. Trans.* **2002**, *43*, 974–983. [[CrossRef](#)]
19. Kaoumi, D.; Liu, J. Deformation induced martensitic transformation in 304 austenitic stainless steel: In-situ vs. ex-situ transmission electron microscopy characterization. *Mater. Sci. Eng. A* **2018**, *715*, 73–82. [[CrossRef](#)]
20. Liu, J.; Kaoumi, D. Use of in-situ TEM to characterize the deformation-induced martensitic transformation in 304 stainless steel at cryogenic temperature. *Mater. Charact.* **2018**, *136*, 331–336. [[CrossRef](#)]
21. Li, N.; Wang, Y.D.; Liu, W.J.; An, Z.N.; Liu, J.P.; Su, R.; Li, J.; Liaw, P.K. In situ X-ray microdiffraction study of deformation-induced phase transformation in 304 austenitic stainless steel. *Acta Metall.* **2014**, *64*, 12–23. [[CrossRef](#)]
22. Zheng, C.S.; Liu, C.J.; Ren, M.H.; Jiang, H.; Li, L.F. Microstructure and mechanical behavior of an AISI 304 austenitic stainless steel prepared by cold-or cryogenic-rolling and annealing. *Mater. Sci. Eng. A* **2018**, *724*, 260–268. [[CrossRef](#)]
23. Talonen, J.; Hänninen, H. Formation of shear bands and strain-induced martensite during plastic deformation of metastable austenitic stainless steels. *Acta Mater.* **2007**, *55*, 6108–6118. [[CrossRef](#)]
24. Stanford, N.; Dunne, D.P. Effect of NbC and TiC precipitation on shape memory in an iron-based alloy. *J. Mater. Sci.* **2006**, *41*, 4883–4891. [[CrossRef](#)]
25. Wang, Y.N.; Chen, J.; Peng, H.B.; Wen, Y.H. Shape memory effect induced by stress-induced α' martensite in a metastable Fe-Cr-Ni austenitic stainless steel. *Acta Metall. Sin. (Engl. Lett.)* **2017**, *30*, 513–520. [[CrossRef](#)]
26. Kruml, T.; Polák, J.; Degallaix, S. Microstructure in 316LN stainless steel fatigued at low temperature. *Mater. Sci. Eng. A* **2000**, *293*, 275–280. [[CrossRef](#)]
27. Lee, W.S.; Lin, C.F. The morphologies and characteristics of impact-induced martensite in 304L stainless steel. *Scr. Mater.* **2000**, *43*, 777–782. [[CrossRef](#)]
28. Sato, K.; Ichinose, M.; Hirotsu, Y.; Inoue, Y. Effects of deformation induced phase transformation and twinning on the mechanical properties of austenitic Fe-Mn-Al alloys. *ISIJ Int.* **1989**, *20*, 868–877. [[CrossRef](#)]
29. Dai, Q.X.; Cheng, X.N.; Luo, X.M.; Zhao, Y.T. Structural parameters of the martensite transformation for austenitic steels. *Mater. Charact.* **2002**, *49*, 367–371. [[CrossRef](#)]

